Gravitational wave imprint of new symmetry breaking*

Wei Chao(晁伟)[1;1)] Wen-Feng Cui(崔文峰)[2,4;2)] Huai-Ke Guo(郭怀珂)[2;3)] Jing Shu(舒菁)[2,3,4;4)]

[1]Center for Advanced Quantum Studies, Department of Physics, Beijing Normal University, Beijing 100875, China
[2]CAS Key Laboratory of Theoretical Physics, Institute of Theoretical Physics, Chinese Academy of Sciences, Beijing 100190, China
[3]CAS Center for Excellence in Particle Physics, Beijing 100049, China
[4]School of Physical Sciences, University of Chinese Academy of Sciences, Beijing 100190, China

Abstract: It is believed that there are more fundamental gauge symmetries beyond those described by the Standard Model of particle physics. The scales of these new gauge symmetries are usually too high to be reachable by particle colliders. Considering that the phase transition (PT) relating to the spontaneous breaking of new gauge symmetries to the electroweak symmetry might be strongly first order, we propose considering the stochastic gravitational waves (GW) arising from this phase transition as an indirect way of detecting these new fundamental gauge symmetries. As an illustration, we explore the possibility of detecting the stochastic GW generated from the PT of $\mathbf{B-L}$ in the space-based interferometer detectors. Our study demonstrates that the GW energy spectrum is reachable by the LISA, Tianqin, Taiji, BBO, and DECIGO experiments only for the case where the spontaneous breaking of $\mathbf{B-L}$ is triggered by at least two electroweak singlet scalars.

Keywords: phase transition, stochastic gravitational waves, **B–L**

DOI: 10.1088/1674-1137/abb4cb

1 Introduction

Although the predictions of the Standard Model (SM) of particle physics agree remarkably well with almost all experimental observations, scientists have not stopped exploring new fundamental gauge symmetries beyond those described by SM, which are usually motivated by the neutrino masses, dark matter, baryon asymmetry of the universe, and the gauge couplings unification at the Grand Unified Theory (GUT). Scales relevant to the spontaneous breaking of new symmetries are usually too high to be accessible by colliders in the foreseeable future. Therefore, how they can be probed is an open question.

The observation of the gravitational wave (GW) signal at the Laser Interferometer Gravitational Wave Observer (LIGO) [1] has opened a new window to explore the universe and various mysteries of particle physics [2-14]. There are usually two sources of GW [4]: (1) cosmological origin, such as inflation and phase transition (PT) and (2) relativistic astrophysical origin, such as binary systems. If PTs related to the spontaneous breaking of the new gauge symmetries are strongly first order, bubbles of the broken phase may nucleate in the background of the symmetric phase when the universe cools down to the bubble nucleation temperature. Bubbles expand, collide, merge, and finally fill the whole universe to finish the PT, and stochastic GW signals can be generated via bubble collisions, sound waves after the bubble collision, and turbulent motion of bulk fluid [15]. We propose considering GW as an indirect way of exploring new gauge symmetries, supposing that the PT of new gauge symmetry breaking is strongly first order.

Considering the complexity of the non-Abelian gauge group extended models, we study GWs generated from PTs of the Abelian gauge group extended models in this paper. There are many possible $U(1)$ extensions of the

Received 9 June 2020, Published online 8 September 2020

* JS is Supported by the National Natural Science Foundation of China (11647601, 11690022, 11675243) and also Supported by the Strategic Priority Research Program of the Chinese Academy of Sciences (XDB23030100). Wei Chao is Supported by the National Natural Science Foundation of China (11775025)

1) E-mail: chaowei@bnu.edu.cn
2) E-mail: cuiwenfeng@itp.ac.cn
3) E-mail: ghk@itp.ac.cn
4) E-mail: jshu@itp.ac.cn

SM [16], of which gauged $\mathbf{B}-\mathbf{L}$ [17-19], $\mathbf{B}$, $\mathbf{L}$ [20-22], $\mathbf{B}+\mathbf{L}$ [23, 24], and $\mathbf{L}_i-\mathbf{L}_j$ [25] (here, $\mathbf{B}$ and $\mathbf{L}$ are the baryon number and lepton number, respectively) have received significant attention. The case of $U(1)_{\mathbf{B}-\mathbf{L}}$ is a relatively minimal extension to the SM for anomaly cancellation and is studied in this work. Notice that the $U(1)_{\mathbf{R}}$ [26], the gauge symmetry for right-handed fermions, shares the same merit as $U(1)_{\mathbf{B}-\mathbf{L}}$ on anomalies cancellation, but this model is severely constrained by the $Z-Z'$ mixing.

We investigate the conditions for the bubble nucleation during the PT of $U(1)_{\mathbf{B}-\mathbf{L}}$ and calculate the energy spectrum of GWs generated from this process. Note that the higher the energy scale of PT, the larger the peak frequency of GW energy spectrum [27]. If $U(1)$ is broken at the TeV scale [28], its GW can be detected at the space-based laser interferometer detectors such as the Laser Interferometer Space Antenna (LISA) [29], Tianqin detector [30], Taiji detector [31], Big Bang Observer (BBO), and DECi-hertz Interferometer Gravitational Wave Observatory (DECIGO) [32]. Alternatively, if $U(1)$ is broken at a scale approaching the GUT, its GW is sensitive to the ground-based laser interferometer such as LIGO. Our results indicate that it is difficult to obtain a large enough GW energy spectrum reachable by the space-based laser interferometer if $\mathbf{B}-\mathbf{L}$ is broken by only one electroweak scalar singlet. Alternatively, if $\mathbf{B}-\mathbf{L}$ is broken by at least two electroweak scalar singlets, its GW energy spectrum is detectable by LISA, Tianqin, Taiji, BBO, and DECIGO. For GWs from the spontaneous breaking of non-Abelian symmetries, we refer the reader to Ref. [33] for the case of the 3-3-1 model [34, 35].

The remainder of the paper is organized as follows: In section 2, we give a brief introduction to the Abelian gauge group extensions to the SM and describe the $U(1)_{\mathbf{B}-\mathbf{L}}$ model in detail. Section 3 discusses the GW signals from the PT of $U(1)_{\mathbf{B}-\mathbf{L}}$. The final section lists concluding remarks.

2 Abelian gauge group extensions to SM

Many $U(1)$ extensions to the SM have been proposed in recent years, often with the motivation of resolving problems in cosmology and astrophysics. There are two ways to construct a gauged $U(1)$ symmetry: top-down approach and bottom-up approach. A typical example of the top-down approach is $U(1)$ from the E_6 GUT [36]. At the GUT scale, E_6 can be broken directly into $SU(3)_C\times SU(2)_L\times U(1)_Y\times U(1)_\psi\times U(1)_\chi$ via the Hosotani mechanism [37]. Some phenomena inspired $U(1)$, such as $\mathbf{L}_i-\mathbf{L}_j$, general $U(1)$ [38], and $U(1)_N$ [39-41], are constructed using the bottom-up approach, whereas $\mathbf{B}-\mathbf{L}$ can be constructed using both approaches. Note that new fermions are needed for the anomaly cancellation of the new Abelian gauge symmetry. Of various $U(1)$ models, $\mathbf{B}-\mathbf{L}$ only requires minimal extensions of the SM with three right-handed neutrinos. Therefore, we study its property of PT and derivative GW spectrum for simplicity. There are usually two types of $\mathbf{B}-\mathbf{L}$ relating to the pattern of symmetry breaking: one electroweak singlet triggered and two electroweak singlets scalar triggered $\mathbf{B}-\mathbf{L}$ breaking. We list the Table 1 patterns of $\mathbf{B}-\mathbf{L}$, particle contents, as well as their charges under $\mathbf{B}-\mathbf{L}$ in Table 1, where N_R represents right-handed neutrino, Φ and Δ are electroweak singlet scalars. In this study, we assume that Φ, Δ, and Z' are heavier than the electroweak scale, such that the PT relating to the new Abelian symmetry and electroweak symmetries breaking can be treated separately.

2.1 Model (a)

The Higgs potential for scenario (a) of $U(1)_{\mathbf{B}-\mathbf{L}}$ can be written as

$$V_0^{(a)}=-\mu_\Phi^2\Phi^\dagger\Phi+\kappa(\Phi^\dagger\Phi)^2, \tag{1}$$

where $\Phi=(\phi+\mathrm{i}G_\Phi+v_\Phi)/\sqrt{2}$, with v_Φ being the vacuum expectation value (VEV) of Φ. The two parameters, μ_ϕ^2 and κ, can be replaced by physical parameters v_ϕ and m_ϕ; $\mu_\phi^2=m_\phi^2/2$, $\kappa=m_\phi^2/2v_\phi^2$. In addition, the Yukawa interactions of N_R are

$$\mathcal{L}_{\mathbf{Y}}\sim y_N\overline{N_R^C}\Phi N_R+y_N\overline{\ell_L}\tilde{H}N_R+\mathrm{h.c.}, \tag{2}$$

where y_N is a 3×3 symmetric Yukawa coupling matrix. The first term generates the Majorana masses for right-handed neutrinos as Φ becomes a nonzero VEV. The tiny but nonzero active neutrino masses arise from the type-I seesaw mechanism [42].

To study properties of the PT, one needs the effective potential at the finite temperature in terms of the background field ϕ,

$$\begin{aligned}V_{\mathrm{eff}}=&V_0+V_{\mathrm{CW}}+V_T+V_{\mathrm{Daisy}}=-\frac{1}{2}\mu_\Phi^2\phi^2+\frac{1}{4}\kappa\phi^4\\&+\frac{1}{64\pi^2}\sum_i(-1)^{2s_i}n_im_i^4(\phi)\left(\log\frac{m_i^2(\phi)}{\mu^2}-C_i\right)\\&+\frac{T^4}{2\pi^2}\left\{\sum_{i\in B}n_iJ_B\left[\frac{m_i^2(\phi)}{T^2}\right]-\sum_{j\in F}n_jJ_F\left[\frac{m_j^2(\phi)}{T^2}\right]\right\}\\&+\frac{T}{12\pi}\sum_i n_i\left\{\left[m_i^2(\phi)\right]^{3/2}-\left[m_i^2(\phi)+\Pi_i(T)\right]^{3/2}\right\},\end{aligned} \tag{3}$$

where V_0 is $V_0^{(a)}$ in terms of the background field; V_{CW}, which is known as the Coleman-Weinberg potential at the zero temperature, containing one-loop contributions to the effective potential at the zero temperature; V_T and V_{Daisy} include the one-loop and the bosonic ring contributions at the finite temperature; n_i and s_i are the number of

Table 1. Quantum numbers of fields under $U(1)_{\rm B-L}$, where Φ and Δ are electroweak scalar singlets.

scenario	Abelian symmetries	Q_L	ℓ_L	U_R	D_R	E_R	N_R	H	Φ	Δ
(a)	$\mathbf{B-L}$	1/3	−1	1/3	1/3	−1	−1	0	2	
(b)	$\mathbf{B-L}$	1/3	−1	1/3	1/3	−1	−1	0	2	1

degrees of freedom and the spin of the ith particle, respectively; C_i equals 5/6 for gauge bosons and 3/2 for scalars and fermions. Eq. (3) is derived in the Landau gauge. It should be noted that the effective potential is gauge dependent, and a gauge invariant treatment of the effective potential is still unknown. We refer the reader to Ref. [43] for a gauge- independent approach to the electroweak PT. Thermal masses of scalar singlet ϕ and gauge boson Z' are given by

$$\Pi_{\phi}^{(a)} = \left(\frac{g_{\mathbf{B-L}}^2}{2} + \frac{\kappa}{3} + \frac{y_N^2}{8}\right)T^2\,, \tag{4}$$

$$\Pi_{Z'}^{(a)} = \frac{5}{3}g_{\mathbf{B-L}}^2 T^2\,, \tag{5}$$

where $g_{\mathbf{B-L}}$ is the gauge coupling of $U(1)_{\mathbf{B-L}}$. In Table 2, we list the field-dependent masses of various particles. One can see from Eq. (3) that the cubic term in the effective potential comes mainly from the loop contribution of Z', such that there is strong correlation between the collider constraints on $g_{\mathbf{B-L}}$, $m_{Z'}$, and the strength of the PT.

2.2 Model (b)

Table 2. Field-dependent masses of various particles.

Scenario (a)		Scenario (b)	
Fields	Masses	Fields	Masses
ϕ	$-\mu_\Phi^2 + 3\kappa\phi^2$	ϕ	$-\mu_\Phi^2 + 3\kappa\phi^2 + \frac{1}{2}\kappa_2\delta^2$
χ	$-\mu_\Phi^2 + \kappa\phi^2$	χ	$-\mu_\Phi^2 + \kappa\phi^2 + \frac{1}{2}\kappa_2\delta^2$
N	$y_{\mathbf{N}}^2\phi^2$	N	$y_{\mathbf{N}}^2\phi^2$
Z'	$4g_{\mathbf{B-L}}^2\phi^2$	Z'	$g_{\mathbf{B-L}}^2(4\phi^2+\delta^2)$
		δ	$-\mu_\Delta^2 + 3\kappa_1\delta^2 + \frac{1}{2}\kappa_2\phi^2$
		χ'	$-\mu_\Delta^2 + \kappa_1\delta^2 + \frac{1}{2}\kappa_2\phi^2$

The correlation of Z' with the PT can be lost in scenario (b), where an extra scalar singlet, $\Delta \equiv (\delta + v_\Delta + {\rm i}\chi')/\sqrt{2}$, is included. For this scenario, the tree-level potential can be written as

$$\begin{aligned} V_0^{(b)} =& -\mu_\Phi^2\Phi^\dagger\Phi + \kappa(\Phi^\dagger\Phi)^2 - \mu_\Delta^2\Delta^\dagger\Delta + \kappa_1(\Delta^\dagger\Delta)^2 \\ &+ \kappa_2(\Phi^\dagger\Phi)(\Delta^\dagger\Delta) + \{\Lambda\Delta^2\Phi^\dagger + {\rm h.c.}\}, \end{aligned} \tag{6}$$

where Λ is a coupling with energy scale. μ_Φ^2 and μ_Δ^2 can be replaced with v_ϕ and v_δ via the tadpole conditions

$$\mu_\phi^2 = \frac{1}{2}\kappa_2 v_\delta^2 + \kappa v_\phi^2 + \frac{\Lambda v_\delta^2}{\sqrt{2}v_\phi}, \tag{7}$$

$$\mu_\Delta^2 = \kappa_1 v_\delta^2 + \frac{1}{2}\kappa_2 v_\phi^2 + \sqrt{2}\Lambda v_\phi. \tag{8}$$

The mass matrix for the CP-even scalars follows

$$\mathcal{M}_{\phi,\delta}^2 = \begin{pmatrix} 2v_\phi^2\kappa - \dfrac{v_\delta^2\Lambda}{\sqrt{2}v_\phi} & v_\delta(v_\phi\kappa_2 + \sqrt{2}\Lambda) \\ v_\delta(v_\phi\kappa_2 + \sqrt{2}\Lambda) & 2v_\delta^2\kappa_1, \end{pmatrix}, \tag{9}$$

which can be diagonalized using a 2×2 orthogonal matrix parametrized by a rotation angle θ,

$$s_1 = c_\theta\phi + s_\theta\delta, \qquad s_2 = -s_\theta\phi + c_\theta\delta, \tag{10}$$

where $s_{1,2}$ are mass eigenstates, with mass eigenvalues m_{s_1} and m_{s_2}, respectively. Three quartic couplings can now be written in terms of physical parameters:

$$\kappa_1 = \frac{m_{s_1}^2 s_\theta^2 + m_{s_2}^2 c_\theta^2}{2v_\theta^2}, \tag{11}$$

$$\kappa_2 = \frac{s_\theta c_\theta(m_{s_1}^2 - m_{s_2}^2) - \sqrt{2}\Lambda v_\delta}{v_\delta v_\phi}, \tag{12}$$

$$\kappa = \frac{2m_{s_1}^2 c_\theta^2 v_\phi + 2m_{s_2}^2 s_\theta^2 v_\phi + \sqrt{2}\Lambda v_\delta^2}{4v_\phi^3}. \tag{13}$$

For the CP-odd scalars, their mass matrix is given by

$$\mathcal{M}_{G_{\phi\chi'}}^2 = -\frac{\Lambda}{\sqrt{2}v_\phi}\begin{pmatrix} v_\delta^2 & -2v_\delta v_\phi \\ -2v_\delta v_\phi & 4v_\phi^2 \end{pmatrix}. \tag{14}$$

It can be diagonalized by a rotation matrix with angle $\theta' = \arctan[v_\delta/(2v_\phi)]$ and gives the following mass eigenstates:

$$G_{Z'} = c_{\theta'}G_\phi + s_{\theta'}\chi', \qquad A = -s_{\theta'}G_\phi + c_{\theta'}\chi', \tag{15}$$

where $G_{Z'}$ is the Goldstone boson, and A is the physical CP-odd scalar with its mass given by $m_A^2 = -\Lambda(v_\delta^2 + 4v_\phi^2)/\sqrt{2}v_\phi$, which implies $\Lambda < 0$. Then, the physical parameters in this scenario are

$$v_\phi, \quad v_\delta, \quad m_{s_1}, \quad m_{s_2}, \quad \theta, \quad \Lambda. \tag{16}$$

The effective potential of scenario (b) has the same form as Eq. (3) up to the following replacements: $(a) \to (b)$, $m_i(\phi) \to m_i(\phi,\delta)$. The field-dependent masses are tabulated in the second column of Table 2. The thermal masses of the various fields are given below:

$$\Pi_{\phi}^{(b)} = \left(\frac{g_{\mathbf{B-L}}^2}{2} + \frac{\kappa}{3} + \frac{\kappa_2}{12} + \frac{y_N^2}{8}\right)T^2\,, \tag{17}$$

$$\Pi_{\delta}^{(b)} = \left(\frac{g_{\mathbf{B-L}}^2}{4} + \frac{\kappa_1}{3} + \frac{\kappa_1}{12}\right)T^2\,, \tag{18}$$

$$\Pi_{Z'}^{(b)} = \frac{7}{4}g_{\mathbf{B-L}}^2 T^2\,. \tag{19}$$

With these inputs, the phase history can be analyzed. A particular advantage of model (b) is that there is a cubic term in Eq. (6) at the tree level, which can generate a barrier between the broken and symmetric phases without the aid of loop corrections. Therefore, it is easier to get a first-order PT for this scenario compared with model (a), where the barrier is provided by Z' from loop corrections.

We now address collider constraints on the Z' mass. A heavy Z' with SM Z couplings to fermions was searched at the LHC in the dilepton channel, which is excluded at the 95% CL for $M_{Z'} < 2.9$ TeV from the ATLAS [44] and for $M_{Z'} < 2.79$ TeV from the CMS [45]. The measurement of $e^+e^- \to f\bar{f}$ above the Z-pole at the LEP-II puts a lower bound on $M_{Z'}/g_{\rm new}$, which is approximately 6 TeV [46]. A further constraint is given by the ATLAS collaboration [47] with 36.1 fb^{-1} of proton-proton collision data collected at $\sqrt{s} = 13$ TeV, which has $M_{Z_{\mathbf{B-L}}} > 4.2$ TeV. We retain these constraints while studying the PTs of these models.

3 Gravitational wave signals

For parameter settings of these two models that can give a first-order phase transition, gravitational waves will be generated, coming mainly from three processes: bubble collisions, sound waves in the plasma, and magnetohydrodynamic turbulence (see Refs. [4, 15, 48] for recent reviews). The total energy spectrum can be written approximately as the sum of these three contributions:

$$\Omega_{\rm GW}h^2 \simeq \Omega_{\rm col}h^2 + \Omega_{\rm sw}h^2 + \Omega_{\rm turb}h^2, \tag{20}$$

where the Hubble constant is defined following the conventional way: $H = 100h\ {\rm kms}^{-1}{\rm Mpc}^{-1}$. The energy spectra depend on three important input parameters for each specific particle physics model: the bubble wall velocity ($\equiv v_w$),

$$\alpha = \left.\frac{\Delta\rho}{\pi^2 g_* T^4/30}\right|_{T=T_n}, \quad \text{and} \quad \beta = H_n T_n \left.\frac{{\rm d}(S_3/T)}{{\rm d}T}\right|_{T=T_n}, \tag{21}$$

where $\Delta\rho$ is the difference in energy densities between the false and true vacua, g_* is the number of relativistic degrees of freedom, and H_n is the Hubble constant evaluated at the nucleation temperature T_n, which corresponds approximately to the temperature when $S_3(T)/T = 140$ [49]. Parameter α characterizes the strength of the PT, whereas β denotes roughly the inverse time duration of the PT. With these parameters solved numerically, one can obtain the energy spectrum of the gravitational waves for the three sources.

First, for the GW from the bubble collision, it can be calculated using the envelop approximation [50-52] by either numerical simulation [53] or recent analytical approximation [54]. Both results can be summarized in the following form:

$$\Omega_{\rm col}h^2 = 1.67\times10^{-5}\Delta(v_w)\left(\frac{H_n}{\beta}\right)^2\left(\frac{\kappa_\phi\alpha}{1+\alpha}\right)^2\left(\frac{100}{g_*}\right)^{1/3}S_{\rm env}(f), \tag{22}$$

where κ_ϕ is the fraction of latent heat transferred to the scalar field gradient, $\Delta(v_w)$ is a numerical factor, and $S_{\rm env}$ captures the spectral shape dependence. The two different treatments by Ref. [54] and Ref. [53] lead to slightly different results of the $\Delta(v_w)$ and $S_{\rm env}$. We adopt the results from the numerical simulation:

$$\Delta(v_w) = \frac{0.48v_w^3}{1+5.3v_w^2+5v_w^4}, \qquad S_{\rm env} = \frac{3.8(f/f_{\rm env})^{2.8}}{1+2.8(f/f_{\rm env})^{3.8}}, \tag{23}$$

with $f_{\rm env}$ i.e., the peak frequency at present time given by

$$f_{\rm env} = 16.5\times10^{-6}\left(\frac{f_*}{\beta}\right)\left(\frac{\beta}{H_n}\right)\left(\frac{T_n}{100{\rm GeV}}\right)\left(\frac{g_*}{100}\right)^{1/6}{\rm Hz}, \tag{24}$$

which is the redshifted frequency of the peak frequency, f_*, at the time of the PT

$$f_* = \frac{0.62}{1.8-0.1v_w+v_w^2}. \tag{25}$$

For the spectral shape $S_{\rm env}$, the analytical treatment in Ref. [54] indicates the correct behavior for low frequency $S_{\rm env} \propto f^3$ required by causality [55], whereas the result from the numerical simulations differs slightly from this one. According to a more recent paper [56], in which the runaway conclusion [57] of the bubble expansion is ruled out, the energy deposited in the scalar field is negligible and should be neglected in GW calculations. Therefore, we neglect the contribution of bubble collision owing to the smallness of κ_ϕ.

Second, the bulk motion of the fluid in the form of the sound wave is produced after bubble collisions. It also generates GWs, and the energy spectrum has been simulated with [58]:

$$\Omega_{\rm sw}h^2 = 2.65\times10^{-6}\left(\frac{H_n}{\beta}\right)^2\left(\frac{\kappa_v\alpha}{1+\alpha}\right)^2\left(\frac{100}{g_*}\right)^{1/3} \times v_w\left(\frac{f}{f_{sw}}\right)^3\left(\frac{7}{4+3(f/f_{\rm sw})^2}\right)^{7/2}, \tag{26}$$

where $f_{\rm sw}$ is the peak frequency at the current time redshifted from the one at the phase transition $2\beta/(\sqrt{3}v_w)$; then,

$$f_{\rm sw} = 1.9\times10^{-5}\frac{1}{v_w}\left(\frac{\beta}{H_n}\right)\left(\frac{T_n}{100{\rm GeV}}\right)\left(\frac{g_*}{100}\right)^{1/6}{\rm Hz}. \tag{27}$$

Similar to κ_ϕ, the factor κ_v is the fraction of latent heat transformed into the bulk motion of the fluid. We use the method summarized in Ref. [59] to calculate κ_v as a function of (α, v_w) and note that a fitted approximate formula is given in Ref. [59]. The above formula is obtained under certain assumptions. It is obtained assuming that the lifetime of the sound waves, τ_v, is one Hubble time [58], i.e., $\tau_v = 1/H_n$, as the gravitational wave spectrum is proportional to $H_n\tau_v$. This leads to $H_n\tau_v \approx 1$ and corresponds to the above result. However, the possible development of shocks and turbulence can happen within one Hubble time and disrupt the gravitational wave generation from sound waves, thus leading to a weaker gravitational wave signal [60]. The time scale for the shocks and turbulence appearance is given roughly by

$$H_n\tau_{\rm sh} \approx \frac{H_nR_*}{\bar{U}_f} = (8\pi)^{1/3}v_w\frac{H_n}{\beta}\frac{1}{\bar{U}_f}, \tag{28}$$

where R_* is the mean bubble separation, which is related to β through the relation $R_* = (8\pi)^{1/3}v_w/\beta$, and $\bar{U}_f$ is the root mean square of the fluid velocity [61]. Therefore, there can be a possible suppression factor $\mathcal{S} \equiv \min(H_n\tau_{\rm sh}, 1)$ [60]. We will consider this factor in the following numerical analysis. Recently, another reduction in gravitational wave generation from sound waves has been observed from numerical simulations [62]. The physical origin of this is the formation of droplets of a metastable phase, which slows down the bubble walls [62]. We will consider its impact when we present more details of the hydrodynamic analysis in later sections. We also note that a more recent numerical simulation by the same collaboration [63] gives a slightly enhanced $\Omega_{\rm sw}h^2$ and a slightly reduced peak frequency $f_{\rm sw}$.

Finally, the plasma at the time of phase transition is fully ionized, and the resulting MHD turbulence can give another source of GWs. Neglecting a possible helical component [64], the generated GW spectrum can be modeled in a similar way [65, 66]:

$$\begin{aligned}\Omega_{\rm turb}h^2 =& 3.35\times10^{-4}\left(\frac{H_n}{\beta}\right)^2\left(\frac{\kappa_{turb}\alpha}{1+\alpha}\right)^{3/2}\left(\frac{100}{g_*}\right)^{1/3}\\ &\times v_w\frac{(f/f_{\rm turb})^3}{[1+(f/f_{\rm turb})]^{11/3}(1+8\pi f/h_*)},\end{aligned} \tag{29}$$

with the peak frequency $f_{\rm turb}$ given by

$$f_{\rm turb} = 2.7\times10^{-5}\frac{1}{v_w}\left(\frac{\beta}{H_n}\right)\left(\frac{T_n}{100{\rm GeV}}\right)\left(\frac{g_*}{100}\right)^{1/6}{\rm Hz}. \tag{30}$$

We need to know factor $\kappa_{\rm turb}$, which is the fraction of latent heat transferred to MHD turbulence. Its precise value is still undetermined, and a recent numerical simulation shows that $\kappa_{\rm turb}$ can be parametrized as $\kappa_{\rm turb} \approx \epsilon\kappa_v$, where numerical factor ϵ varies roughly in the range of 5% ~ 10% [58]. In this study, $\epsilon = 0.1$ tentatively.

For the detection of GWs, one needs to compare these spectra with the sensitivity curve of each detector. The LISA detector is currently the most mature experiment, and the recently finished LISA pathfinder has confirmed its design goals. Therefore, we consider the sensitivities of the LISA configuration N2A5M5L6(C1) presented in Refs. [15, 67], which include the instrumental noise of the LISA detector obtained using the detector simulation package LISACode [68] as well as the astrophysical foreground from the compact white dwarf binaries in our galaxy. We also consider the discovery prospect of several other proposed experiments: Tianqin, Taiji, BBO, DECIGO, [1] and Ultimate-DECIGO [69] (UDECIGO).

We implement two $\mathbf{B}-\mathbf{L}$ models in CosmoTransitions [70], which traces the phase history of each model, locates the critical temperature T_C, and gives the bounce solutions to obtain the bubble nucleation temperature T_n. We then use these outputs to calculate the GW energy spectra and compare them with the listed detector sensitivities.

From an extensive scan over the parameter space of model (a) at the mass scale of O(TeV), we find that a first-order PT can occur for a significant proportion of their parameter spaces. However, the resulting GW signals are generally too weak to be discovered, where the most optimistic case can marginally be reached by the Ultimate-DECIGO. This is due to the relatively large values of β and small values of α obtained, aside from the enhanced O(TeV) temperature, which reduces the magnitude of GW energy spectrum as well as pushes the peak frequency to higher values. On the other hand, for the parameter space at the electroweak scale, the GWs can generally be reached by most detectors, which is however ruled out by collider searches of Z'.

Model (b) has a sizable parameter space, where the generated GWs from PT fall within the sensitive regions of various detectors owing to the easily realized PT from the tree level barrier with the aid of a negative cubic term in the effective potential in Eq. (6). We demonstrate a benchmark point from this parameter space and present the details of the PT and the GW spectrum. This benchmark parameter point is $v_\phi = 4637$ GeV, $v_\delta = 1902$ GeV, $\theta = 0.128$, $m_{s_1} = 2400$ GeV, $m_{s_2} = 1236$ GeV, and $\Lambda = -2143$ GeV. For this case, the minima in the field space (ϕ,δ) lie in direction $\phi > 0$, where the cubic term in Eq. (6) is negative. Owing to the reflection symmetry $\delta \to -\delta$, it occurs in a pair. The shape of the effective potential is depicted as contours in Fig. 1, where hot regions have larger values of V, whereas cold regions have smaller values. The left figure depicts the shape at a relatively high temperature where the universe sits at its ori-

1) The BBO and DECIGO sensitivity data are taken from the website http://rhcole.com/apps/GWplotter/

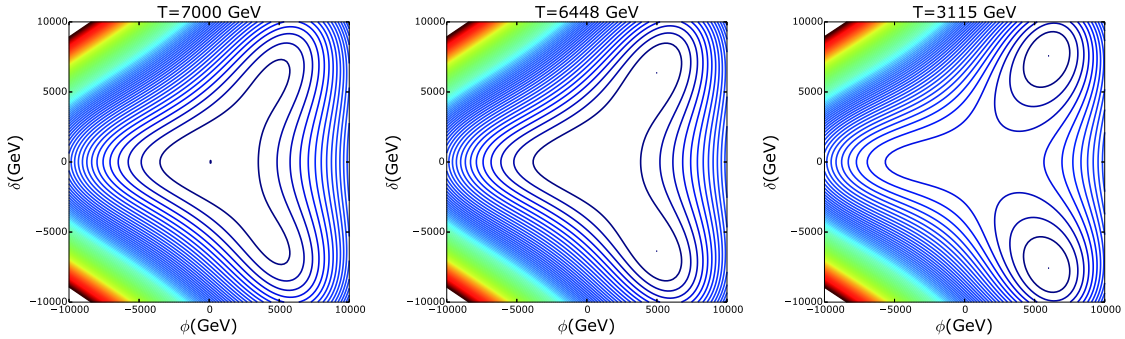

Fig. 1. (color online) Contours of the effective potential of model (b) at three typical temperatures, with blue lines for lower values and red for higher values. The left figure is at a temperature higher than $T_C \approx 6448$ GeV, the middle one is at T_C, and the right figure is at $T_n \approx 3115$ GeV. The benchmark parameters are: $v_\phi = 4637$ GeV, $v_\delta = 1902$ GeV, $\theta = 0.128$, $m_{s_1} = 2400$ GeV, $m_{s_2} = 1236$ GeV, and $\Lambda = -2143$ GeV.

gin and the two minima in direction $\phi > 0$ are developing. As T drops to the critical temperature $T_C \approx 6448$ GeV, these two minima become degenerate with the one at the origin, as exhibited in the middle figure. As T drops further below the critical temperature, the broken phase begins to nucleate on the background of symmetric phase at $T_n \approx 3115$ GeV, which is depicted in the right figure. The details of the evolution of the new phase are presented in Fig. 2 in plane (ϕ,δ), where the arrow denotes the direction of time flow and the colors indicate the value of temperature. Note that T_n differs noticeably from T_n, indicating a significant amount of supercooling. However, as we will see later, α is still relatively small, and there is no intermediate inflationary stage, and the phase transition can be safely completed.

To calculate the GWs from this model, we need the input κ_v, which we calculate following Ref. [59]. For the benchmark given in Fig. 1, we find $\alpha = 0.09$, $\beta/H_n \approx 6$, and κ_v depending on one free parameter v_w. For different values of v_w, the motion of the plasma surrounding the bubble takes different forms, and the value of κ_v is shown in the left panel of Fig. 3, where representative points are marked as A, B, C, and D, shown as green points in the figure. The velocity profile of the plasma is depicted in the right panel of Fig. 3 as a function of r/t, where r is the radial distance from the bubble center and t starts at T_n. For case A, v_w is smaller than the speed of sound in the plasma ($\equiv c_s = 1/\sqrt{3}$, the vertical dashed line in left panel), and the bubble proceeds as deflagrations, with a velocity profile shown by the dotted lines in the right panel. For case B, v_w is larger than c_s, a rarefaction wave develops behind the bubble wall, yet the fluid has nonzero velocity ahead of the wall, indicated as the solid lines in the right panel. This falls within the hybrid region of the left panel, denoting supersonic deflagration [71]. For case C, v_w is increased to the Jouguet detonation [72] (the magenta dotted line in the left panel) and the velocity of the fluid ahead of the wall becomes zero, indicated as the dashed line in the right panel. For case D,

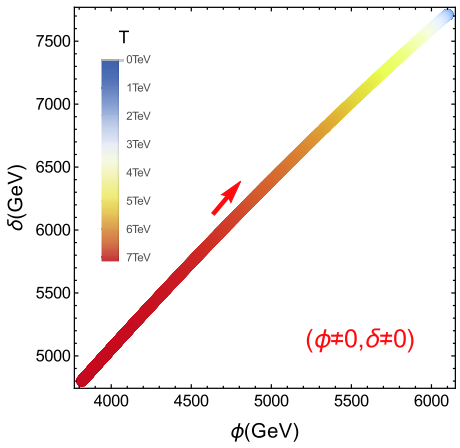

Fig. 2. (color online) Tracks of the minimum $(\phi \neq 0,\ \delta \neq 0)$ in the (ϕ,δ) plane, with the colors indicating the value of temperature, which can be read from the colormap on the left.

the bubble wall velocity becomes larger and the expansion takes the form of detonation with the profile depicted by the dot-dashed line in the right panel. For these four choices of v_w, we find $\bar{U}_f \approx 0.12$, 0.09, 0.09, and 0.07, respectively. From Eq. (28), it follows that $H_n\tau_{\rm sh} \approx 1.56$, 3.24, 4.03, and 5.85, respectively. Because all these values are larger than 1, there is no need to consider the suppression caused by the early onset of shocks and turbulence. For smaller values of v_w, $H_n\tau_{\rm sh}$ decreases. More precisely, for this choice of α, we have $H_n\tau_{\rm sh} < 1$ when $v_w < 0.25$, and one needs to consider this suppression. The other reduction effect, found in Ref. [62], is small for these benchmarks, because α is small (see Fig. 6 of Ref. [62] or see Fig. 2 of Ref. [73] for this reduction factor on the (v_w,α) plane).

The resulting GW energy spectra for these four points from sound waves (blue dashed) and turbulence (brown dotted) are depicted in Fig. 4, where their sum corresponds to the red solid line. The color-shaded regions at the top are the experimental sensitivity regions for the LISA configurations C1 (red), Tianqin (yellow), Taiji

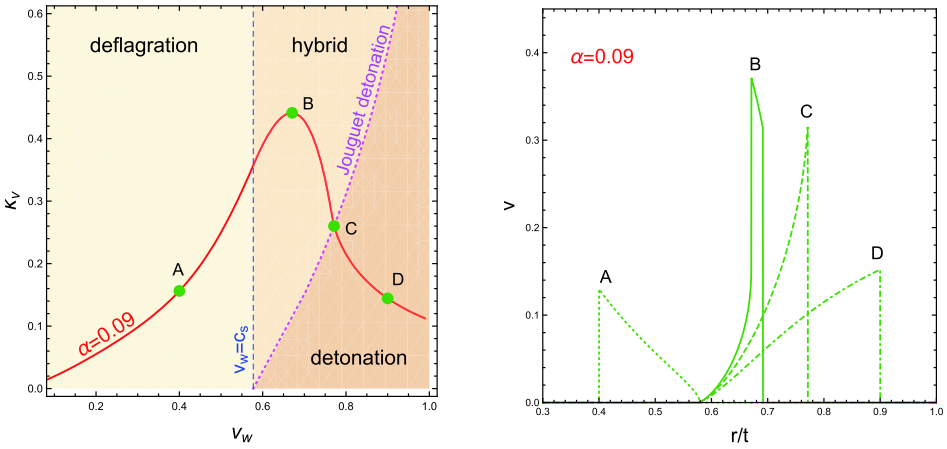

Fig. 3. (color online) Left panel: The red line shows the fraction of latent heat transferred to the bulk motion of the plasma κ_v when the bubble wall velocity is varied for $\alpha = 0.09$, which is derived the benchmark in Fig. 1. Also plotted here are the deflagration, hybrid(supersonic deflagration), and detonation regions characterizing the dynamics of the phase transition, separated by the blue dashed line (when v_w is equal to the speed of sound of the relativistic plasma $c_s = 1/\sqrt{3}$) and the magenta dotted line (Jouguet detonation). Four representative cases: A, B, C and D, marked with green points, are chosen to calculate the GW spectra. Right panel: The velocity profile as a function of r/t for the four representative cases of the left panel plot.

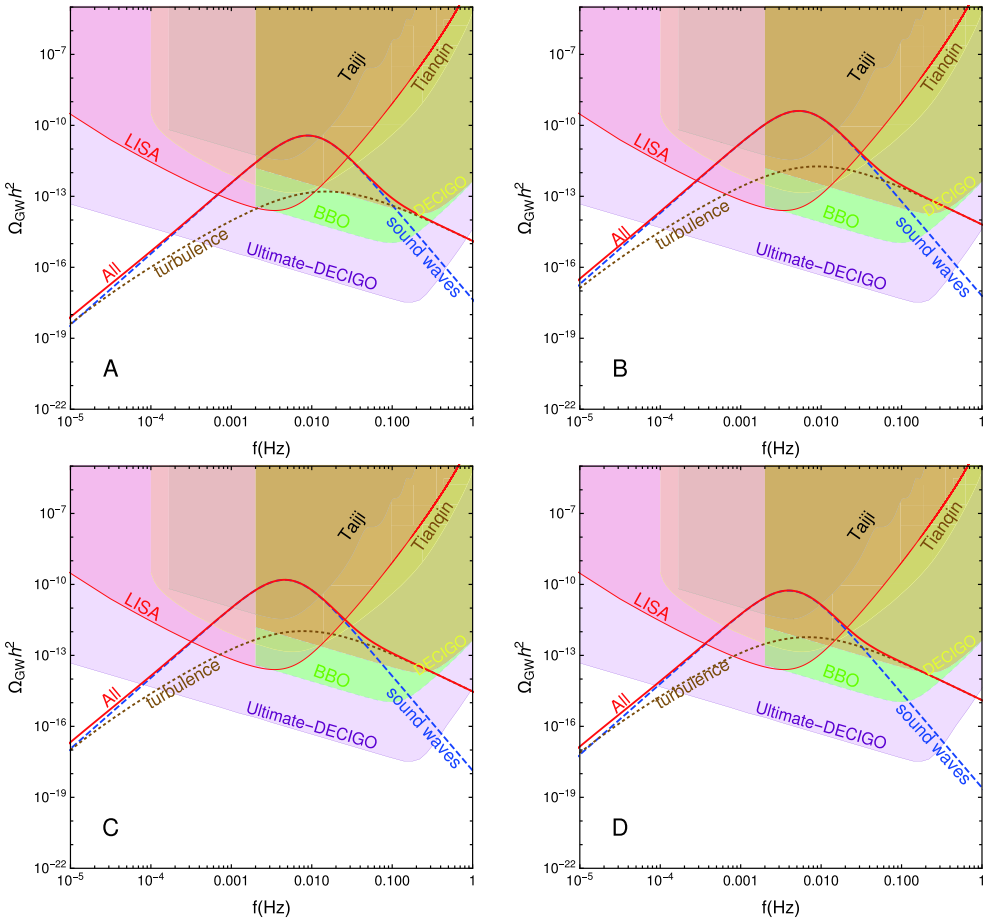

Fig. 4. (color online) GW energy spectrum as function of its frequency for the benchmark in Fig. 1, and four representative bubble wall velocities (the four green points A, B, C, and D in Fig. 3). The individual contributions from sound waves and turbulence are plotted using blue dashed and brown dotted lines, respectively, with their sum given as the red solid line. Also plotted are the experimental sensitive regions at the top, corresponding to color-shaded regions, from the LISA detector with C1 configuration, Tianqin (yellow), Taiji (gray), DECIGO (brown), BBO (green), and Ultimate-DECIGO(purple).

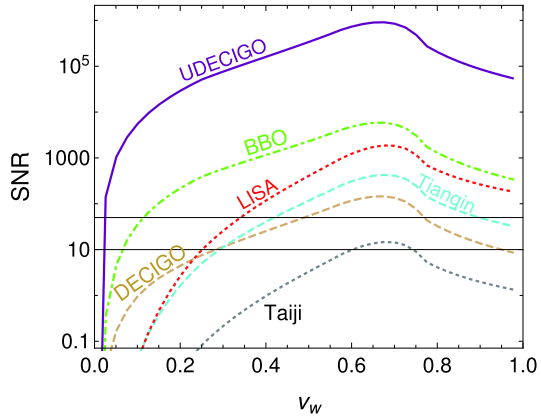

Fig. 5. (color online) SNR as function of bubble wall velocity v_w for the benchmark point in model (b) using the different experimental sensitivity inputs. Two black horizontal lines denote SNR threshold values of 10 and 50, respectively.

(gray), DECIGO (brown), BBO (green), and Ultimate-DECIGO (purple). It is observed that, for all four cases, the spectrum at around the peak frequency is dominated by sound waves, whereas turbulence becomes more important for large and small frequencies. The total GW spectra all fall within the experimental sensitive regions of the LISA configuration as well as other experiments. To assess the discovery prospect of the GWs, we quantify the detectability of the GWs using the signal-to-noise ratio adopted in Ref. [15]:

$$\mathrm{SNR} = \sqrt{\mathcal{T}\int_{f_{\min}}^{f_{\max}} \mathrm{d}f \left[\frac{h^2\Omega_{\mathrm{GW}}(f)}{h^2\Omega_{\mathrm{exp}}(f)}\right]^2}\,, \tag{31}$$

where $h^2\Omega_{\mathrm{exp}}$ is the experimental sensitivity depicted in Fig. 4 and $\mathcal{T}$ is the mission duration of the experiment in years. For all cases, we set $\mathcal{T} = 5$. With this formula, we calculate SNR as a function of v_w for each experiment and present the results in Fig. 5. Note that v_w can take the full range of values between 0 and 1. One needs to check the suppression factor $\mathcal{S}$. As discussed earlier, this affects mainly the region $v_w \lesssim 0.25$ for this choice of α and leads to a slight reduction in the gravitational wave signal and thus the SNR. We incorporate this suppression in our calculations. For the other reduction as recently observed in Ref. [62], its effect is minor because α is quite small and is neglected in this study. We also demonstrate two representative SNR thresholds $\mathrm{SNR}_{\mathrm{thr}} = 10, 50$ as suggested by Ref. [15] with horizontal black lines for comparison. From this figure, we can see that all SNR curves have a peak at $v_w \approx 0.67$. This peak corresponds to the maximum of $\kappa_v \approx 0.44$ in the left panel of Fig. 3, represented by case B in previous discussion, which has a supersonic deflagration profile of the plasma surrounding the bubble. It is clear from this figure that, for a wide range of v_w, the SNR for the LISA configuration C1, Tianqin, BBO, and UDECIGO are above the two thresholds $\mathrm{SNR}_{\mathrm{thr}} = 10, 50$. For DECIGO, there is also a range $0.5 \lesssim v_w < 0.8$ above threshold 50, and this range becomes much wider for threshold 10. For Taiji, there is a window at $v_w \approx 0.7$ where the SNR is above 10. We note that these SNRs are obtained assuming a mission duration of 5 years. Also note that the used sensitivity curves depend on the specific detector configurations proposed, such as the arm length and noice level achieved. All these are subject to change if the eventual configurations are changed.

4 Discussion

The discovery of GW at LIGO heralds a new era in high-energy physics and gravity. In this paper, we proposed the stochastic GW as an indirect way of probing the spontaneous breaking new gauge symmetry beyond the SM. Working with models with the gauged $\mathbf{B}-\mathbf{L}$ extension of the SM, we studied the strength of PT relating to the spontaneous breaking of the $\mathbf{B}-\mathbf{L}$ as well as the stochastic GW signals generated during the same PT in the space-based interferometer. We found that the power spectrum of GW generated is reachable by LISA, Tianqin, Taiji, BBO, DECIGO, and Ultimate-DECIGO for the case where the spontaneous breaking of $\mathbf{B}-\mathbf{L}$ is triggered by at least two electroweak scalar singlets. It should be mentioned that there is no way to identify its intrinsic physics if any stochastic GW signal is observed. However, it provides a guidance for new physics hunters because the stochastic GW signal with peak frequency at near 0.01 Hz hints at new scalar interactions or new symmetry at the TeV scale. This study makes sense of this point of view. Although we focused only on the $U(1)$ case in this study, our results can be easily extended to the non-Abelian case because it contains all ingredients of the GW calculation.

References

1 B. P. Abbott *et al.*, Phys. Rev., **X6**(4): 041015 (2016), arXiv:1606.04856
2 I. P. Ivanov, Prog. Part. Nucl. Phys., **95**: 160-208 (2017), arXiv:1702.03776
3 A. Beniwal, M. Lewicki, J. D. Wells *et al.*, *Gravitational wave, collider and dark matter signals from a scalar singlet electroweak baryogenesis*, arXiv: 1702.06124
4 R.-G. Cai, Z. Cao, Z.-K. Guo *et al.*, *The Gravitational-Wave Physics*, arXiv: 1703.00187, doi: 10.1093/nsr/nwx029
5 A. Addazi and A. Marciano, *Gravitational waves from dark first order phase transitions and dark photons,* arXiv: 1703.03248
6 K. Tsumura, M. Yamada, and Y. Yamaguchi, *Gravitational wave from dark sector with dark pion,* arXiv: 1704.00219, doi: 10.1088/1475-7516/2017/07/044

7 Z. Kang, P. Ko, T. Matsui, *Strong First Order EWPT and Strong Gravitational Waves in Z_3-symmetric Singlet Scalar Extension,* arXiv: 1706.09721
8 W. Chao, Phys. Lett. B, **796**: 102-106 (2019), arXiv:1706.01041
9 L. Bian, H.-K. Guo, and J. Shu, *Gravitational Waves, baryon asymmetry of the universe and electric dipole moment in the CP-violating NMSSM*, arXiv: 1704.02488
10 F. P. Huang and J.-H. Yu, *Explore Inert Dark Matter Blind Spots with Gravitational Wave Signatures*, arXiv: 1704.04201
11 A. Addazi and A. Marciano, *Limiting Majoron self-interactions from Gravitational waves experiments*, arXiv: 1705.08346
12 L. Marzola, A. Racioppi, and V. Vaskonen, Eur. Phys. J. C, **77**(7): 484 (2017), arXiv:1704.01034
13 C.-W. Chiang and E. Senaha, *On gauge dependence of gravitational waves from a firstorder phase transition in classical scale-invariant U(1)' models*, arXiv: 1707.06765
14 W. Chao, H.-K. Guo, and J. Shu, JCAP, **09**: 009 (2017), arXiv:1702.02698
15 C. Caprini *et al*., JCAP, **1604**(04): 001 (2016), arXiv:1512.06239
16 P. Langacker, Rev. Mod. Phys., **81**: 1199-1228 (2009), arXiv:0801.1345
17 R. N. Mohapatra and R. E. Marshak, Phys. Rev. Lett., **44**: 1316 (1980), [Erratum: Phys. Rev. Lett., **44**: 1643 (1980)], doi: 10.1103/PhysRevLett.44.1316
18 R. E. Marshak and R. N. Mohapatra, Phys. Lett. B, **91**: 222-224 (1980)
19 C. Wetterich, Nucl. Phys. B, **187**: 343-375 (1981)
20 P. Fileviez Perez and M. B. Wise, Phys. Rev. D, **82**: 011901 (2010), [Erratum: Phys. Rev. D, **82**: 079901 (2010)], arXiv: 1002.1754, doi: 10.1103/PhysRevD.82.079901, 10.1103/PhysRevD.82.011901
21 T. R. Dulaney, P. Fileviez Perez, and M. B. Wise, Phys. Rev. D, **83**: 023520 (2011), arXiv:1005.0617
22 W. Chao, Phys. Lett. B, **695**: 157-161 (2011), arXiv:1005.1024
23 W. Chao, Phys. Rev. D, **93**(11): 115013 (2016), arXiv:1512.06297
24 W. Chao, H.-k. Guo, and Y. Zhang, JHEP, **04**: 034 (2017), arXiv:1604.01771
25 X.-G. He, G. C. Joshi, H. Lew *et al*., Phys. Rev. D, **44**: 2118-2132 (1991)
26 W. Chao, *Phenomenology of the gauge symmetry for right-handed fermions*, arXiv: 1707.07858
27 P. S. B. Dev and A. Mazumdar, Phys. Rev. D, **93**(10): 104001 (2016), arXiv:1602.04203
28 F. P. Huang, Y. Wan, D.-G. Wang *et al*., Phys. Rev. D, **94**(4): 041702 (2016), arXiv:1601.01640
29 H. Audley *et al*., *Laser Interferometer Space Antenna*, arXiv: 1702.00786
30 J. Luo *et al*., Class. Quant. Grav., **33**(3): 035010 (2016), arXiv:1512.02076
31 X. Gong *et al*., J. Phys. Conf. Ser., **610**(1): 012011 (2015), arXiv:1410.7296
32 K. Yagi and N. Seto, Phys. Rev. D, **83**: 044011 (2011), [Erratum: Phys. Rev. D, **95**: 109901 (2017)], arXiv: 1101.3940, doi: 10.1103/PhysRevD.83.044011
33 F. P. Huang and X. Zhang, *Probing the hidden gauge symmetry breaking through the phase transition gravitational waves,* arXiv: 1701.04338
34 F. Pisano and V. Pleitez, Phys. Rev. D, **46**: 410-417 (1992), arXiv:hep-ph/9206242
35 P. H. Frampton, Phys. Rev. Lett., **69**: 2889-2891 (1992)
36 S. F. King, S. Moretti, and R. Nevzorov, Phys. Rev. D, **73**: 035009 (2006), arXiv:hep-ph/0510419
37 Y. Hosotani, Phys. Lett. B, **126**: 309-313 (1983)
38 T. Appelquist, B. A. Dobrescu, and A. R. Hopper, Phys. Rev. D, **68**: 035012 (2003), arXiv:hep-ph/0212073
39 W. Chao, Int. J. Mod. Phys. A, **30**(01): 1550007 (2015), arXiv:1202.6394
40 W. Chao and M. J. Ramsey-Musolf, Phys. Rev. D, **89**(3): 033007 (2014), arXiv:1212.5709
41 Y. Cai and W. Chao, Phys. Lett. B, **749**: 458-463 (2015), arXiv:1408.6064
42 P. Minkowski, Phys. Lett. B, **67**: 421-428 (1977)
43 H. H. Patel and M. J. Ramsey-Musolf, JHEP, **07**: 029 (2011), arXiv:1101.4665
44 G. Aad *et al*., Phys. Rev. D, **90**(5): 052005 (2014), arXiv:1405.4123
45 V. Khachatryan *et al*., JHEP, **04**: 025 (2015), arXiv:1412.6302
46 M. Carena, A. Daleo, B. A. Dobrescu *et al*., Phys. Rev. D, **70**: 093009 (2004), arXiv:hep-ph/0408098
47 M. Aaboud *et al*., *Search for new high-mass phenomena in the dilepton final state using 36.1 fb^{-1} of proton-proton collision data at $\sqrt{s}$ = 13 TeV with the ATLAS detector*, arXiv: 1707.02424
48 D. J. Weir, *Gravitational waves from a first order electroweak phase transition: a review*, 2017. arXiv: 1705.01783. URL http://inspirehep.net/record/1598112/files/arXiv:1705.01783.pdf
49 R. Apreda, M. Maggiore, A. Nicolis *et al*., Nucl. Phys. B, **631**: 342-368 (2002), arXiv:gr-qc/0107033
50 A. Kosowsky, M. S. Turner, and R. Watkins, Phys. Rev. D, **45**: 4514-4535 (1992)
51 A. Kosowsky, M. S. Turner, and R. Watkins, Phys. Rev. Lett., **69**: 2026-2029 (1992)
52 A. Kosowsky and M. S. Turner, Phys. Rev. D, **47**: 4372-4391 (1993), arXiv:astro-ph/9211004
53 S. J. Huber and T. Konstandin, JCAP, **0809**: 022 (2008), arXiv:0806.1828
54 R. Jinno and M. Takimoto, Phys. Rev. D, **95**(2): 024009 (2017), arXiv:1605.01403
55 C. Caprini, R. Durrer, T. Konstandin *et al*., Phys. Rev. D, **79**: 083519 (2009), arXiv:0901.1661
56 D. Bodeker and G. D. Moore, JCAP, **1705**(05): 025 (2017), arXiv:1703.08215
57 D. Bodeker and G. D. Moore, JCAP, **0905**: 009 (2009), arXiv:0903.4099
58 M. Hindmarsh, S. J. Huber, K. Rummukainen *et al*., Phys. Rev. D, **92**(12): 123009 (2015), arXiv:1504.03291
59 J. R. Espinosa, T. Konstandin, J. M. No *et al*., JCAP, **1006**: 028 (2010), arXiv:1004.4187
60 J. Ellis, M. Lewicki, and J. M. No, *Gravitational waves from first-order cosmological phase transitions: lifetime of the sound wave source,* arXiv: 2003.07360
61 M. Hindmarsh and M. Hijazi, JCAP, **12**: 062 (2019), arXiv:1909.10040
62 D. Cutting, M. Hindmarsh, and D. J. Weir, *Vorticity, kinetic energy, and suppressed gravitational wave production in strong first order phase transitions*, arXiv: 1906.00480
63 M. Hindmarsh, S. J. Huber, K. Rummukainen *et al*., *Shape of the acoustic gravitational wave power spectrum from a first order phase transition*, arXiv: 1704.05871
64 T. Kahniashvili, L. Campanelli, G. Gogoberidze *et al*., Phys. Rev. D, **78**: 123006 (2008), [Erratum: Phys. Rev. D, **79**: 109901 (2009)], arXiv: 0809.1899, doi: 10.1103/PhysRevD.78.123006, 10.1103/PhysRevD.79.109901
65 C. Caprini, R. Durrer, and G. Servant, JCAP, **0912**: 024 (2009), arXiv:0909.0622
66 P. Binetruy, A. Bohe, C. Caprini *et al*., JCAP, **1206**: 027 (2012), arXiv:1201.0983
67 A. Klein *et al*., Phys. Rev. D, **93**(2): 024003 (2016), arXiv:1511.05581
68 A. Petiteau, G. Auger, H. Halloin *et al*., Phys. Rev. D, **77**: 023002 (2008), arXiv:0802.2023
69 H. Kudoh, A. Taruya, T. Hiramatsu *et al*., Phys. Rev. D, **73**: 064006 (2006), arXiv:gr-qc/0511145
70 C. L. Wainwright, Comput. Phys. Commun., **183**: 2006-2013 (2012), arXiv:1109.4189
71 H. Kurki-Suonio and M. Laine, Phys. Rev. D, **51**: 5431-5437 (1995), arXiv:hep-ph/9501216
72 P. J. Steinhardt, Phys. Rev. D, **25**: 2074 (1982)
73 A. Alves, D. Gonalves, T. Ghosh *et al*., JHEP, **03**: 053 (2020), arXiv:1909.05268